Piezo-transmissive Structure using Multi-Layered Heterogeneous Film for Optical Transmittance Modulation

Gihun Lee [1†], Jungrak Choi[1†], Junseong Ahn[1], Seokju Cho[1], and Inkyu Park[1,]*

[1] Department of Mechanical Engineering, Korea Advanced Institute of Science and Technology (KAIST), 291 Daehak-ro, Yuseong-gu, Daejeon, 305-701, South Korea

ABSTRACT

As the damage caused by the recent climate crisis increases, efforts are being made to develop low-power and high-efficiency technologies to reduce pollution for energy production worldwide. Among them, research on mechano-responsive optical transmittance modulation technology is being actively conducted as it can be applied to various application fields for reducing energy consumption: low-power sensors and smart windows. The piezo-transmittance structure, which is one of the optical transmittance modulation structures, has fewer constraints on the installation environment, thereby many applications have been proposed. However, it is still challenging to fabricate a piezo-transmittance structure with large area production, high throughput, and good tunability because of complex curing and dissolution processes. Herein, we present an efficient fabrication method for a multi-layered piezo-transmittance structure using a large area abrasive mold and thermal imprinting process. The piezo-transmittance performance (e.g. sensitivity and relative change of transmittance) shows temperature/humidity-independent characteristics and can be designed by tuning design parameters such as the number of layers, abrasive grade, and film material. Also, the surrogate model of the performance obtained from the Monte Carlo simulation and prediction model can offer tunability for various applications. Finally, we demonstrated two energy-efficient applications; The smart window integrated with a hydraulic pump showed high thermal efficiency in indoor environment control, and the telemetry system was demonstrated to measure pressure remotely.

Keywords: multi-layered structure, abrasive, thermal imprinting, piezo-transmittance, smart window, telemetry

INTRODUCTION

Recently, with the advancement of internet of things (IoT) technology, various sensors and electrical devices are increasingly being used in various applications ranging from large places[1-3] (e.g. factories, buildings) to human body[4-6]. However, as the energy required to operate numerous systems also increases, low-power[7-9] and high-efficiency[10-12] technologies have attracted significant interests to respond to the current severe climate and energy crisis. In this background, studies related to the optical transmittance modulation technology with good energy-saving properties have been actively conducted. The technology refers to a technology in which a structure's coloration or light transmittance is changed by an external stimulus such as electrical, thermal, and mechanical stimuli. The technology includes electrochromic[13-15], thermochromic[16-18], polymer dispersed liquid crystal[19-21], and mechanoresponsive types. Among them, the mechano-responsive optical transmittance modulation technology in which the transmittance is changed by the physical deformation (i.e. strain and pressure) has shown many advantages: a large transmittance change, fast response to actuators, and small energy to maintain a transmittance state.[22-24] Based on these advantages, the structure can be integrated into zero energy building or car tint to selectively control light transmittance for regulating indoor environment with low energy consumption. Furthermore, some researchers introduced that the structure can be used as two types of physical sensors[25,26], to establish low-power wearable sensor systems. However, strain-induced structures have to be attached to the surface, so unexpected behavior such as sliding friction occurs due to contact constraints. For practical applications ranging from smart windows to sensors, pressure-induced structure, which is also called “piezo-transmittance structure”, can be more appropriate than the strain-induced structure because strain-induced structures require attachment to a

surface and can experience unexpected behavior, such as sliding friction, due to contact constraints. On the other hand, the contact constraint problems associated with sliding and friction can be avoided by pressure-induced structures. Among piezo-transmittance structure, porous structures have been adopted in many studies owing to their high sensitivity and simple fabrication methods. Choi *et al*. achieved high sensitivity and large transmittance change by combination of an organic solar cell and porous elastomer structure[27] made using sub-cm sized sugar cube template[28,29]. However, template-based fabrication method takes time to cure elastomer and dissolve template by solvent, and the piezo-transmittance performance design parameters are limited to the material due to the fixed geometry of the template. Also, the fixed geometry of commercial templates causes difficulties for large-area fabrication. A large-area process is possible when a porous structure is produced by directly mixing particles (sugar, salt, Polystyrene (PS) beads, etc.) with the base material[30-32]. Bilent *et al.* adjusted the ratio of PDMS and sugar particles[45], and Kang *et al.* adjusted the size of PS particles[44] to tune piezo-transmittance performances, yet there are low throughput and waste problems. In addition, theoretical prediction and design of the performance is difficult because of random arrangement in 3D, thereby the optimization has been performed empirically. Lastly, the method using a blowing agent[33-35] is the most commercially suitable method, which enables large-area fabrication and exhibits high throughput. But there is a limit to the thickness reduction since a cutting process is necessary. Therefore, methodologies for the design with a desired operation conditions and high-throughput fabrication of large area specimen are required.

Herein, we introduce a cost-effective, simple, and tunable piezo-transmittance structure named “Multi-layered heterogenous film (MLHF)” based on multiple layers of heterogeneous films: low-modulus rough film and high-modulus flat film. The structure stacked with rough film thermally patterned using an abrasive has a similar mechanism to the

conventional porous structure. In comparison to previous approaches that relied on silicone elastomers and various fabrication methods of porous structures, our structure and method with various parametric studies according to the Young's modulus, number of layers, refractive index of flat film, and grade of abrasive possess distinct advantages in terms of cost-effectiveness and practicality for industrial mass production. The MLHF is fabricated by a thermal imprinting process, enabling a large-area fabrication with high-fidelity pattern replication, high throughput, and low waste[36-38]. In addition, the MLHF exhibits an sensitive piezo-transmittance response within the smart window (zero-energy building, car tint, smart farm, etc.) and sensor operating temperature and humidity ranges. A Monte-Carlo simulation and an analytical model were applied to obtain a predictive model for the piezo-transmittance behavior of MLHF, and the surrogate model was created for the range of changes in transmittance and sensitivity. Finally, we demonstrated two applications integrated with the MLHF structure designed by surrogate model-based optimization process: a smart window with a hydraulic actuator, and a remote monitoring system using a camera capable of continuously measuring temperature, humidity, and pressure.

RESULTS AND DISSCUSION

Figure 1a shows a schematic illustration of the working principle of MLHF. The rough surface imprinted with an abrasive induces a lot of light scattering under low-pressure loading conditions, and this leads to lengthening of effective optical path within the structure and significant light attenuation according to the Beer-Lambert law. In addition, only a small portion of light rays reach the detector while a majority of rays are scattered in all directions. As a result, it shows higher optical transmittance by increasing the applied pressure. By the same mechanisms, the image of the target object becomes clearer by increasing the applied pressure. The design parameters of the MLHF are the grade of the abrasive, number of layers,

and material (Young's modulus, and refractive index), as shown in Figure 1b. The piezo-transmittance performance according to design parameters was predicted by the surrogate modeling. Figure 1c shows applications of the MLHF: a remote monitoring system using a camera (i) and human eyes (ii), and a smart window (iii). The MLHF's tunability allows applications ranging from remote monitoring to measure blast pressure to smart windows with the principle previously mentioned. In remote monitoring system applications, by using ambient light such as sunlight as a light source and measuring pressure through a camera or eyes, it is possible to realize a low-power or no-power consumption system. In smart window applications, MLHF is capable of efficient temperature control by controlling light transmittance. The thermal imprinting process using a laminator makes it possible to manufacture large-area MLHF for smart windows with a size of several tens of centimeters. Compared to the conventional fabrication method which contains a template dissolution process, semi-permanently usable mold is applied, which has the advantage of less waste and reduces the time required for curing and dissolving template.

Figure 2a shows a schematic illustration of the MLHF fabrication process with 2 steps: thermal imprinting for adhesion of two heterogeneous films and patterning by abrasive, and multilayer lamination of several unit layers. For flat films, polycarbonate (PC), methyl methacrylate (PMMA), polyethylene terephthalate (PET), etc. with high modulus are applied, and rough films are composed of thermoplastic polyurethane (TPU) or styrene-ethylene-butylene-styrene (SEBS) with low elastic moduli. The MLHF can be fabricated as a product with a sufficiently large area as shown in Figure 2b. In Figure 2c, the microscope image shows a cross-section of the MLHF fabricated in the form of 8 layers (SEBS-PET). Figure 2d shows the confocal microscope image and the SEM image of the surface profile of the rough film. The undercuts shown in the SEM image allow high sensitivity performance over a wide pressure range, as mentioned in the previous research[46]. The pattern produced through the

thermal imprinting process was evaluated with a similar quality as those fabricated by casting or hot-press method (See Figure S3 and Table S3 for details).

A compression test was performed to analyze the piezo-transmittance behavior of the MLHF with various design parameters such as the number of layers, Young's modulus, refractive index, and the grade of abrasive. Figure 3a is the result of the parameter study according to the grade of the abrasive. The types of abrasives selected for the parameter study are P600, P1000, and P2000. The larger the grade the smaller the standard deviation of the slope (Table S4). The pattern of P600 initially exhibits low transmittance but it increases rapidly with pressure as shown in Figure S4a (the initial transmittance (T_0) of each MLHF is 0.16, 0.27, and 0.373 in ascending order of grade). A large standard deviation of a surface gradient distribution with the zero-mean means that the rays are more likely to collide with a structure with a large gradient, bringing about more scattering effects. The relative change of transmittance ($\Delta T/T_0$) for P600, P1000, and P2000 under 5 MPa condition was observed as 0.88, 1.51, and 2.47, respectively. Thus, it can be inferred that the smaller the grade of the abrasive, the larger the relative change of transmittance and the sensitivity characteristics. In Fig. 3b and Table S5, increasing the number of layers seems to enhance the relative change of transmittance more effectively, as the transmittance changes 7.5 times larger than the initial transmittance for 12 layers. As the number of layers increases, the number of light scattering events increases, lowering the initial transmittance. As the overall thickness of MLHF decreases by applying a pressure, the transmittance increases accordingly. Figure 3c shows the relationship between the refractive indices of the flat film and rough film. No significant effect of refractive index could be observed under the experimental conditions of this study. The effect of the Young's modulus is the greatest on the piezo-transmittance behavior of the MLHF as shown in Figure 3d. SEBS (54kPa) has much smaller Young's modulus than TPU (3.4MPa) and operates in a low-pressure range (~100's kPa), while MLHF composed of TPU operates in a high-pressure range

(~10MPa). Therefore, it seems likely that the design of the MLHF should be in the order of selecting the suitable material for the approximate pressure range and then finely controlling the remaining parameters such as number of layers and grade of abrasive. Figure 3e and Figure 3f show that the initial transmittance and normalized sensitivity of MLHF made of SEBS and PET are not highly dependent on the temperature and relative humidity, in the temperature range of 20-75℃ and the relative humidity range of 10-70%. It has been confirmed that MLHF can be used stably within the harsh conditions of the environment where MLHF will be applied, such as car tints and smart windows in buildings. Especially, SEBS, in which the glass transition temperatures of the butadiene and styrene blocks are 183K and 373K, respectively, seem to have small changes of flexural modulus in the real range for applications between the glass transition temperatures.

According to Persson's study[39] which presented the relationship between the ratio of the area flattened on a rough surface and the pressure, the larger the variance of the slope in the surface profile, the lower the sensitivity of the piezo-transmittance performance. However, as a result of the parameter study on grade, the larger the variance of the slope in the surface profile exists, the larger the range of transmittance change is observed. As such, it is necessary to acquire a surrogate model to improve both the sensitivity and range of transmittance change, which are performance indicators considered when designing MLHF. A predictive model was established as shown in Figure 4a to estimate the performance of the MLHF's range of transmittance change and sensitivity depending on the design parameters. The initial transmittance of the predictive model was obtained through Monte-Carlo simulation with a ray tracing simulation (See Figure S5 for details) for the deterministic model (See Figure S6 for details), and the subsequent behavior was obtained through the analytical model (See Figure S7 for details). Helseth's research, which confirmed that the transmittance of one rough layer is proportional to the ratio of the flattened area[40], was extended to the MLHF analytical model including Beer-

Lambert law and Fresnel equation. The predictive model includes two strategies for computational efficiency. The 2D model simulation greatly reduces the amount of computation that occurs in the intersection search algorithm, and the assumption about ignoring secondary rays reduces the number of rays that need to be traced. Second, the analytical model reduces the effort on structural analysis and ray tracing simulations performed on the surface at each pressure. The predictive model can approximate the behavior of MLHF while consuming little computing time as shown in Figure 4b. As shown in Figure S7, the assumption that light transmits only on a flat surface makes some error in the low-pressure range, and the error caused by the assumption decreases as the pressure increases. Due to the limitations of the analytical model, the transmittance of the low-pressure region is underestimated, but it would be efficient for securing sufficient data for generating a surrogate model. The shallow artificial neural network model (Figure S8) that can reflect the nonlinearity of the model was used to obtain the surrogate model of transmittance change and sensitivity and shows the excellent regression result (R=0.9963) in Figure 4c. The output of the surrogate model was defined as the weighted summation of the range of transmittance change and sensitivity. Figure 4d shows the effect of each input variable (refractive index difference, the number of layers, the grade of the abrasive, rough film thickness) on sensitivity and range of transmittance change through the F-test-based feature importance analysis during the acquisition of the surrogate model. It appears that the number of layers is the most sensitive parameter for designing the MLHF. It was also observed that the transmittance at high pressures (above 5 MPa) tended to converge as shown in Fig. S4a-c. Judging from the parameter study results, it is important how much the initial transmittance can be lowered, and the number of layers appears to be a variable that effectively lowers the initial transmittance. When integrated into smart windows, MLHF should have high pressure sensitivity and large range of transmittance change for low actuation power and higher thermal transmission/insulation switching performance, respectively. In

addition, large range of transmittance change can enhance the resolution of pressure in a remote pressure monitoring system. Therefore, design optimization was performed to minimize the cost function (maximize the sensitivity and the range of transmittance change) obtained through the surrogate modeling, and the compression test result for the optimal MLHF is depicted in Figure 4e. The initial transmittance of optimal MLHF is about 1.5%, and it has an excellent range of transmittance change ($\Delta T = 84\%$) and sensitivity ($\frac{dT}{dP} = 0.0047kPa^{-1}$). Optimized MLHF was applied to the smart window and remote pressure monitoring system.

Figure 5a is a schematic diagram of the effect of smart windows integrated with MLHF. In general, the structure can control the amount of heat radiation from the light, reducing the effort required for temperature control in various applications. In the case of MLHF, it is expected that an additional thermal insulation effect may occur due to the air gap with a very low heat conductivity ($0.025 W/m \cdot K$). Figure 5b (i) shows the system configuration of the smart window including a solenoid valve and a hydraulic pump. The solenoid valve minimizes the power required to maintain the state of the smart window, and the hydraulic pump allows to effectively control the transmittance over and arbitrarily sized and curved surfaces. Each result when the MLHF structure applied to smart window is released and compressed is shown in Figure 5b (ii). The enhanced thermal isolation performance of MLHF is confirmed in Figure 5c. The time spent for heating from 30 to 45℃ and cooling from 45 to 30℃ of the normal window, pressurized MLHF, and MLHF in a released state were measured. When the MLHF covered on the chamber's window was fully pressurized and released, a 5°C heating took ~15% and ~500% longer, respectively, compared to the bare window. On the other hand, cooling took ~65% and ~463% longer, respectively. These results reflect that MLHF has potential as a smart window because it can effectively control the thermal insulation performance. Compared to other optical transmittance modulation technologies such as thermochromic[16-18] and polymer

dispersed liquid crystal[19-21] type, which consume power to maintain the state of light transmittance, MLHF might have the advantage of low-power consumption in an environment where transmittance modulation is not frequent (See Table S8 for details).

Pressure monitoring is required in a wide range of applications such as air pressure or structural pressure monitoring from daily life to dangerous environment. Figure 6a shows the principle of a remote pressure monitoring system. The image blurred by the rough surface of the MLHF is gradually sharpened by the increased pressure. The remote monitoring system, which monitors pressure through the normalized cross correlation coefficient (NCC) between the image to which MLHF is applied and the reference image, was demonstrated (See details in Figure S9). As shown in Figure 6b, the proposed telemetry system can have the advantages of ensuring the safety of equipment and human from harsh conditions (i), and easy installation and measurement (ii). Figure 6c shows the relationship between the pressure and NCC, and it might be seen that pressure can be estimated using remote images taken by the camera. Three images were applied to figure out the effect of images on NCC. One image contains a black (value of 0 in grayscale) circle with an area of $0.79\ \mathrm{cm}^2$ on a white (value of 255 in grayscale) background, another image contains a black circle with an area of $3.16\ \mathrm{cm}^2$ on the same background, and the other image contains 4 black circles with an area of $0.79\ \mathrm{cm}^2$ for each circle. As a result, it was observed that the NCC difference was large in proportion to the area of the black circle on the white background. The image with a black area of $3.16\ \mathrm{cm}^2$showed an NCC difference of about 0.8 in the range of 0 to $1\ \mathrm{MPa}$, and the image with a black area of $0.79\ \mathrm{cm}^2$ showed an NCC difference of about 0.5. Since the camera image shows mostly a white-colored image in a situation where no pressure is applied, it can be inferred that the ratio of black pixels in a picture which is used as the reference must be increased to generate a large NCC difference. Furthermore, the testing of triangular, circular, and rectangular images of the same area showed similar pressure-NCC curves, indicating a relatively small effect of

image shape on the system's performance (Figure S10). From the result in Figure 6d, the remote pressure monitoring system showed a stable response in a cyclic pressure test (4,000 cycles).

CONCLUSION

In this study, MLHF, which consists of soft rough films fabricated by thermal imprinting on abrasive and flat films with relatively higher modulus, was developed to provide optical transmittance modulation by pressure, and used for smart window and telemetry applications. Initial transmittance is low due to light scattering and long effective path length which are induced by the rough film. Increasing the pressure makes soft rough film flattened and raises the optical transmittance. The advantages of the thermal imprinting process, such as low manufacturing waste and mass producibility, were confirmed through fabrication results. Based on the parametric study, the tunability of the MLHF through the design parameters (i.e. number of layers, refractive index of the film, abrasive grade and Young's modulus) was confirmed. It also exhibited high stability over the temperature and humidity operating range of the application. Through a predictive model and ray tracing simulation based on Persson’s theory, a surrogate model of MLHF according to the refractive index difference, the number of layers, film thickness, and type of abrasive was created. Based on the design optimization process using the surrogate model, MLHF with high sensitivity and range of transmittance change were designed and applied to smart window and remote pressure sensing system. Based on the demonstration of smart window application, MLHF can lead to excellent insulation with low heat radiation and thermal conductivity by air. In addition, usage of hydraulic pump and solenoid pump reduces required power to maintain modulated transmittance. The remote pressure sensing system with MLHF and camera can measure the pressure without power of light source and communication module. We believe that the MLHF will make a significant contribution in various applications where low-power and high-efficiency systems are required.

To the best of our knowledge, this is the first piezo-transmittance structure with practical characteristics such as large area fabrication and tunability in the field of mechano-responsive optical transmittance modulation technology technology. It is expected to have a great impact on various fields such as wearable sensors, environmental sensors, and smart windows with its self-powered and thermal insulation characteristics. In addition, compared to the porous structure that accounts for the majority of piezo-transmittance structure, the design of MLHF relies on a surrogate model to quantify piezo-transmittance performance, providing a quantitative rather than empirical design basis. If a material with a lower Young's modulus than the material used in this study or a surface profile with higher sensitivity is applied, it will be possible to design an MLHF operating in much lower pressure range. This will lower the power required for the smart window operation and improve the resolution of the remote pressure sensing system.

EXPERIMENTAL SECTION

Preparation of MLHF fabrication. PC (20 % (w/v)), SEBS (60 % (w/v)), and PMMA solutions were used for a thin film deposition process using a knife coater (Knife coating device 3000, KIBAE Inc., Korea). PC (PC film, AS ONE Inc., Japan) was dissolved in chloroform ($CHCl_3$, 98.5%, Sigma Aldrich), and SEBS was dissolved in toluene ($C_6H_5CH_3$, 99.8%, Sigma Aldrich), and PMMA solution (495 PMMA A5, KAYAKU Co., Ltd, Japan) was used. After bar coating, chloroform and toluene were evaporated at room temperature, and coated PMMA film was heated at 80℃ for 5 minutes. TPU film (VB1085, Ventwin Inc., Korea) and PET film were prepared as commercial products in the form of rolls. All films fabricated by the bar coating process were produced on PET substrates (Coating Q film, Formetc Inc., Korea). After laminating the film and the abrasive mold of less than 2500 grit (Silicon carbide abrasive,

CC261, Deerfos Inc., Korea) or the abrasive mold of 2500 grit or more (Silicon carbide abrasive, 991A, Matador Inc., Germany), thermoforming was performed using a laminator (Excelam Ⅱ -355Q, GMP Inc., Korea) at 130℃.

Characterization of the MLHF. The morphology of the cross-section of MLHF was characterized using an optical microscope (VHX-500F, KEYENCE, Japan). The 3D surface morphologies and profiles of the rough film were measured using a 3D laser scanning confocal microscope (VX-X1050, KETENCE, Japan), and analyzed using MATLAB (Figure S2 and Table S2). To evaluate the young's moduli of SEBS and TPU, their specimens were manufactured according to ASTM D412 standard, and evaluated using a high-precision universal testing machine (AGS-X, SHIMADZU, Japan) (Figure S1). The refractive indices of materials from the references were used [41,42]. The molar absorption coefficients of materials were measured using a UV/VIS spectrophotometer (Lambda 650, PerkinElmer Inc., USA) and the average value was obtained in the visible light region (400nm ~ 700nm) (Table S1). Static and dynamic response characteristics of MLHF were measured by a load cell (WLS-300LCK, CAS Korea, Korea) with a linear stage (SAS, SAMICK THK, Korea), which was used for displacement control and measurement, and a photodiode sensor (S120C, Thorlabs, USA). The source of light was a solar illuminator (LAX-C100 Xenon light source, Asahi Spectra Co., Ltd., Inc., Japan). To conduct environmental tests, temperature and humidity sensors (BME280, Bosch Sensortec, Germany) were integrated and measured, and the environment was controlled with a PTC heater and humidifier.

Surrogate modeling and design optimization process of the MLHF. The surrogate modeling

and design optimization process were all performed using MATLAB. Surface profiles acquired using the laser confocal microscope were expanded through a random surface generation algorithm43. The transmittance under no pressure (P=0) was obtained through Monte-Carlo simulation with a ray tracing algorithm. 100,000 collimated rays were randomly sampled (uniform distribution) in one simulation. Conditions to which pressure was applied (P>0) were obtained using the analytical model, and the transmittance in the Monte-Carlo simulation and the transmittance in the analytical model at very high pressure (P=10 MPa) were used as boundary conditions. Inputs (refractive index difference, number of layers, grade, and rough film thickness) to be applied to the predictive model for generating a surrogate model were extracted through the Latin hypercube sampling method in the range as shown in Table S6. The sensitivity and range of transmittance change data for 1000 designs obtained through the predictive model were regressed using a shallow neural network. Using the obtained surrogate model, the design optimization process by applying the inter-point algorithm to the bounds shown in Table S7 was carried out. The overall system thickness was less than 1mm as a nonlinear constraint.

Fabrication of the smart window with MLHF, and experimental equipment. The dimensions of MLHF obtained through design optimization for the smart window are shown in Table S4. MLHF with an area of 5cm×5cm was sandwiched between acrylic plates with an area of 12cm×12cm, and then placed in a plastic bag. The pressure inside the plastic bag is regulated via a solenoid valve (KAB21-02-02-12V, KCC Co, LTD., Korea), a vacuum pump (FAS20-1, FALCON Inc., USA), and an Arduino mega IoT device. Also, Arduino mega measured temperature and humidity using a BME280 sensor. A halogen lamp was used for

heating.

Fabrication of the remote monitoring system with MLHF. The dimensions of MLHF obtained through design optimization for the remote monitoring system are the same as the dimensions of MLHF of the smart window. A temperature indicator strip (Artmagics Co., Korea) and a humidity indicator strip (ONESTEP Inc., China) were added to the reference and sensing images. The code for the remote monitoring system was written based on Python's OpenCV library. The hardware of the remote monitoring system consists of Raspberry Pi 4 and its camera module (8MP Camera module V2) (Figure S8).

ASSOCIATED CONTENT

Supporting Information.

The Supporting Information is available free of charge on the ACS Publications website at DOI:

Details regarding the material properties; Abrasive mold and pattern profile analysis; Supporting results of parameter study; Details regarding the design optimization process and results including predictive model and surrogate model; Configuration of remote pressure monitoring system and its algorithm; (PDF)

Transmittance modulation of the smart window using a hydraulic pump (MP4)

Demonstration of the remote monitoring system with MLHF (MP4)

AUTHOR INFORMATION

Corresponding Authors

*E-mail: inkyu@kaist.ac.kr

ORCID : 0000-0001-5761-7739

Notes

The authors declare no competing financial interest.

ACKNOWLEDGEMENTS

G. Lee [1†] and J. Choi[1†] contributed equally to this study. (1) This work was supported by the National Research Foundation of Korea (NRF) grant funded by the Korea government (MSIT) (No. 2021R1A2C3008742). (2) This research was also supported by Ministry of Culture, Sports and Tourism and Korea Creative Content Agency (Project Number: R2021040018).

ORCID

Gihun Lee : 0000-0001-7281-3092
Jungrak Choi : 0000-0001-6049-7504
Junseong Ahn : 0000-0002-4090-5440
Seokju Cho : 0000-0001-5499-1266
Inkyu Park : 0000-0001-5761-7739 ✔

REFERENCES

(1) Waters, M.; Waszczuk, P.; Ayre, R.; Dreze, A.; McGlinchey, D.; Alkali, B.; Morison, G. Open Source IIoT Solution for Gas Waste Monitoring in Smart Factory. *Sensors* **2022**, 22, No. 2972.

(2) Dong, B.; Prakash, V.; Feng, F.; O'Neill, Z. A review of smart building sensing system for better indoor environment control. *Energ. Buildings* **2019**, 199, 29-46.

(3) Muangprathub, J.; Boonnam, N.; Kajornkasirat, S.; Lekbangpong, N.; Wanichsombat, A.; Nillaor, P. IoT and Agriculture Data Analysis for Smart Farm. *Comput. Electron. Agr.* **2019**, 156, 467-474.

(4) Ruth, S. R. A.; Feig, V. R.; Tran, H.; Bao, Z. N. Microengineering Pressure Sensor Active Layers for Improved Performance. *Adv. Funct. Mater.* **2020**, *30*, No. 2003491.

(5) Jung, Y.; Choi, J.; Lee, W.; Ko, J. S.; Park, I.; Cho, H. Irregular Microdome Structure-Based Sensitive Pressure Sensor Using Internal Popping of Microspheres. *Adv. Funct. Mater.* **2022**, 32, No. 2201147.

(6) Yang, J. C.; Mun, J.; Kwon, S. Y.; Park, S.; Bao, Z. N.; Park, S. Electronic Skin: Recent Progress and Future Prospects for Skin-Attachable Devices for Health Monitoring, Robotics, and Prosthetics. *Adv. Mater.* **2019**, 31, No. 1904765.

(7) Dong, K.; Peng, X.; Cheng, R.; Ning, C.; Jiang, Y.; Zhang, Y.; Wang, Z. L. Advances in High-Performance Autonomous Energy and Self-Powered Sensing Textiles with Novel 3D Fabric Structures. *Adv. Mater.* **2022**, 34, No. 2109355.

(8) Luo, J.; Wang, Z.; Xu, L.; Wang, A. C.; Han, K.; Jiang, T.; Lai, Q.; Bai, Y.; Tang, W.; Fan, F. R.; et al. Flexible and Durable Wood-based Triboelectric Nanogenerators for Self-powered Sensing in Athletic Big Data Analytics. *Nat. Commun.* **2019**, 10, 5147.

(9) Ahn, J.; Kim, J. S.; Jeong, Y.; Hwang, S.; Yoo, H.; Jeong, Y.; Gu, J.; Mahato, M.; Ko, J.; Jeon, S.; et al. All-Recyclable Triboelectric Nanogenerator for Sustainable Ocean Monitoring Systems. *Adv. Energy. Mater.* **2022**, 12, No. 2201341.

(10) Lee, D. K.; Park, N. G. Materials and Methods for High-Efficiency Perovskite Solar Modules. *Sol. Rrl.* **2022**, 6, No. 2100455

(11) Tusnina, V.; Tusnin, A.; Alekperov, R. Experimental and Theoretical Studies of the Thermal Efficiency of Multilayer Non-Uniform Building Enclosures. *J. Build. Eng.* **2022**, 45, No. 103439.

(12) Lin, X. C.; Sun, X.; Manogaran, G.; Rawal, B. S. Advanced Energy Consumption System for Smart Farm Based on Reactive Energy Utilization Technologies. *Environ. Impact. Asses.* **2021**, No. 106496.

(13) Azam, A.; Kim, J.; Park, J.; Novak, T. G.; Tiwari, A. P.; Song, S. H.; Kim, B.; Jeon, S. Two-Dimensional Wo3 Nanosheets Chemically Converted from Layered Ws2 for High-Performance Electrochromic Devices. *Nano. Lett.* **2018**, 18, 5646-5651.

(14) Liu, Z. X.; Yang, J. Y.; Leftheriotis, G.; Huang, H.; Xia, Y.; Gan, Y. P.; Zhang, W. K.; Zhang, J. A Solar-Powered Multifunctional and Multimode Electrochromic Smart Window Based on Wo3/Prussian Blue Complementary Structure. *Sustain. Mater. Techno.* **2022**, 31, No. 00372.

(15) Chen, J. W.; Tan, A. W. M.; Eh, A. L. S.; Lee, P. S. Scalable Inkjet Printing of Electrochromic Smart Windows for Building Energy Modulation. *Adv. Energ. Sust. Res.* **2022**, 3, No. 2100172.

(16) Zhang, J.; Wang, J.; Yang, C. M.; Jia, H. B.; Cui, X. M.; Zhao, S. C.; Xu, Y. Mesoporous Sio2/Vo2 Double-Layer Thermochromic Coating with Improved Visible Transmittance for Smart Window. *Sol. Energ. Mat. Sol. C* **2017**, 162, 134-141.

(17) Long, S. W.; Cao, X.; Sun, G. Y.; Li, N.; Chang, T. C.; Shao, Z. W.; Jin, P. Effects of V2o3 Buffer Layers on Sputtered Vo2 Smart Windows: Improved Thermochromic Properties, Tunable Width of Hysteresis Loops and Enhanced Durability. *Appl. Surf. Sci.* **2018**, 441, 764-772.

(18) Zhang, Q. H.; Jiang, Y. W.; Chen, L. T.; Chen, W.; Li, J. X.; Cai, Y. F.; Ma, C. Q.; Xu, W. H.; Lu, Y. Q.; Jia, X. D.; et al. Ultra-Compliant and Tough Thermochromic Polymer for Self-Regulated Smart Windows. *Adv. Funct. Mater.* **2021**, 31, No. 2100686.

(19) Hemaida, A.; Ghosh, A.; Sundaram, S.; Mallick, T. K. Evaluation of Thermal Performance for a Smart Switchable Adaptive Polymer Dispersed Liquid Crystal (Pdlc) Glazing. *Sol. Energy* **2020**, 195, 185-193.

(20) Ghosh, A.; Mallick, T. K. Evaluation of Optical Properties and Protection Factors of a Pdlc Switchable Glazing for Low Energy Building Integration. *Sol. Energ. Mat. Sol. C* **2018**, 176, 391-396.

(21) Wu, Y.; Cao, H.; Duan, M. Y.; Li, E. L.; Wang, H. H.; Yang, Z.; Wang, D.; He, W. L. Effects of a Chemically Modified Multiwall Carbon Nanotubes on Electro-Optical Properties of Pdlc Films. *Liq. Cryst.* **2018**, 45, 1023-1031.

(22) Yu, H. F.; Dong, C.; Zhou, W. M.; Kobayashi, T.; Yang, H. A. Wrinkled Liquid-Crystalline Microparticle-Enhanced Photoresponse of Pdlc-Like Films by Coupling with Mechanical Stretching. *Small* **2011**, 7, 3039-3045.

(23) Lee, E.; Zhang, M. L.; Cho, Y.; Cui, Y.; Van der Spiegel, J.; Engheta, N.; Yang, S. Tilted Pillars on Wrinkled Elastomers as a Reversibly Tunable Optical Window. *Adv. Mater.* **2014**, 26, 4127-4133.

(24) Cho, D.; Shim, Y. S.; Jung, J. W.; Nam, S. H.; Min, S.; Lee, S. E.; Ham, Y.; Lee, K.; Park, J.; Shin, J.; et al. High-Contrast Optical Modulation from Strain-Induced Nanogaps at 3d Heterogeneous Interfaces. *Adv. Sci.* **2020**, 7, No.1903708.

(25) Ge, D. T.; Lee, E.; Yang, L. L.; Cho, Y. G.; Li, M.; Gianola, D. S.; Yang, S. A Robust Smart Window: Reversibly Switching from High Transparency to Angle-Independent Structural Color Display. *Adv. Mater.* **2015**, 27, 2489-2495.

(26) Gu, J. M.; Ahn, J.; Jung, J. Y.; Cho, S.; Choi, J.; Jeong, Y.; Park, J.; Hwang, S.; Cho, I.; Ko, J.; et al. Self-Powered Strain Sensor Based on the Piezo-Transmittance of a Mechanical Metamaterial. *Nano Energy* **2021**, 89, No. 106447.

(27) Choi, J.; Kwon, D.; Kim, B.; Kang, K.; Gu, J. M.; Jo, J.; Na, K.; Ahn, J.; Del Orbe, D.; Kim, K.; et al. Wearable Self-Powered Pressure Sensor by Integration of Piezo-Transmittance Microporous Elastomer with Organic Solar Cell. *Nano Energy* **2020**, 74, No. 104749.

(28) Choi, J.; Kwon, D.; Kim, K.; Park, J.; Del Orbe, D.; Gu, J.; Ahn, J.; Cho, I.; Jeong, Y.; Oh, Y.; et al. Synergetic Effect of Porous Elastomer and Percolation of Carbon Nanotube Filler toward High Performance Capacitive Pressure Sensors. *Acs. Appl. Mater. Inter.* **2020**, 12, 1698-1706.

(29) Hwang, K.; Ahn, J.; Cho, I.; Kang, K.; Kim, K.; Choi, J.; Polychronopoulou, K.; Park, I. Microporous Elastomer Filter Coated with Metal Organic Frameworks for Improved Selectivity and Stability of Metal Oxide Gas Sensors. *Acs Appl Mater Inter* **2020**, 12, 13338-13347.

(30) Kang, S. B.; Lee, J.; Lee, S.; Kim, S.; Kim, J. K.; Algadi, H.; Al-Sayari, S.; Kim, D. E.; Kim, D.; Lee, T. Highly Sensitive Pressure Sensor Based on Bioinspired Porous Structure for Real-Time Tactile Sensing. *Adv. Electron. Mater.* **2016**, 2, No. 1600356.

(31) Yang, J. C.; Kim, J. O.; Oh, J.; Kwon, S. Y.; Sim, J. Y.; Kim, D. W.; Choi, H. B.; Park, S. Microstructured Porous Pyramid-Based Ultrahigh Sensitive Pressure Sensor Insensitive to Strain and Temperature. *Acs. Appl. Mater. Inter.* **2019**, 11, 19472-19480.

(32) Wang, S. Z.; Almenabawy, S. M.; Kherani, N. P.; Leung, S. N.; O'Brien, P. G. Solar-Driven Interfacial Water Evaporation Using Open-Porous Pdms Embedded with Carbon Nanoparticles. *Acs. Appl. Energ. Mater.* **2020**, 3, 3378-3386.

(33) Tsivintzelis, I.; Pavlidou, E.; Panayiotou, C. Biodegradable Polymer Foams Prepared with Supercritical Co2-Ethanol Mixtures as Blowing Agents. *J. Supercrit. Fluid* **2007**, 42, 265-272.

(34) Grande, J. B.; Fawcett, A. S.; McLaughlin, A. J.; Gonzaga, F.; Bender, T. P.; Brook, M. A. Anhydrous Formation of Foamed Silicone Elastomers Using the Piers-Rubinsztajn Reaction. *Polymer* **2012**, 53, 3135-3142.

(35) Tebboth, M.; Jiang, Q. X.; Kogelbauer, A.; Bismarck, A. Inflatable Elastomeric Macroporous Polymers Synthesized from Medium Internal Phase Emulsion Templates. *Acs. Appl. Mater. Inter.* **2015**, 7, 19243-19250.

(36) Lan, S. H.; Song, J. H.; Lee, M. G.; Ni, J.; Lee, N. K.; Lee, H. J. Continuous Roll-to-Flat Thermal Imprinting Process for Large-Area Micro-Pattern Replication on Polymer Substrate. *Microelectron. Eng.* **2010**, 87, 2596-2601.

(37) Retolaza, A.; Juarros, A.; Ramiro, J.; Merino, S. Thermal Roll to Roll Nanoimprint Lithography for Micropillars Fabrication on Thermoplastics. *Microelectron. Eng.* **2018**, 193, 54-61.

(38) Yi, P. Y.; Deng, Y. J.; Shu, Y. Y.; Peng, L. F. Experimental Studies on a Novel Roll-to-Roll Powder Hot Embossing for Large-Area Fabrication of Micropyramid Arrays on Polymers. *J. Micromech. Microeng.* **2018**, 28, No. 085007.

(39) Emami, A.; Khaleghian, S.; Taheri, S. Asperity-Based Modification on Theory of Contact Mechanics and Rubber Friction for Self-Affine Fractal Surfaces. *Friction* **2021**, 9, 1707-1725.

(40) Helseth, L. E. Optical Force Sensing Principle Based on Transparent Elastomer with a Rough Surface. *Sensor. Actuat. a-Phys.* **2017**, 263, 667-676.

(41) Ahmad, Z.; Kumar, K. D.; Saroop, M.; Preschilla, N.; Biswas, A.; Bellare, J. R.; Bhowmick, A. K. Highly Transparent Thermoplastic Elastomer from Isotactic Polypropylene and Styrene/Ethylene-Butylene/Styrene Triblock Copolymer: Structure-Property Correlations. *Polym. Eng. Sci.* **2010**, 50, 331-341.

(42) Brissinger, D. Complex Refractive Index of Polycarbonate over the Uv-Vis-Ir Region from 0.2 to 3 Mu M. *Appl. Optics.* **2019**, 58, 1341-1350.

(43) Pawlus, P.; Reizer, R.; Wieczorowski, M. A Review of Methods of Random Surface Topography Modeling. *Tribol. Int.* **2020**, 152, No. 106530.

(44) Kang, S. B.; Lee, J.; Lee, S.; Kim, S.; Kim, J. K.; Algadi, H.; Al-Sayari, S.; Kim, D. E.; Kim, D.; Lee, T. Highly Sensitive Pressure Sensor Based on Bioinspired Porous Structure for Real-Time Tactile Sensing. *Adv. Electron. Mater.* **2016**, 2, No. 1600356.

(45) Bilent, S.; Dinh, T. H. N.; Martincic, E.; Joubert, P. Y. Influence of the Porosity of Polymer Foams on the Performances of Capacitive Flexible Pressure Sensors. *Sensors* **2019**, 19, No. 1968.

(46) Bai, N. N.; Wang, L.; Wang, Q.; Deng, J.; Wang, Y.; Lu, P.; Huang, J.; Li, G.; Zhang, Y.; Yang, J. L.; et al. Graded Intrafillable Architecture-Based Iontronic Pressure Sensor with Ultra-Broad-Range High Sensitivity. *Nature Communications* **2020**, 11, No. 209.

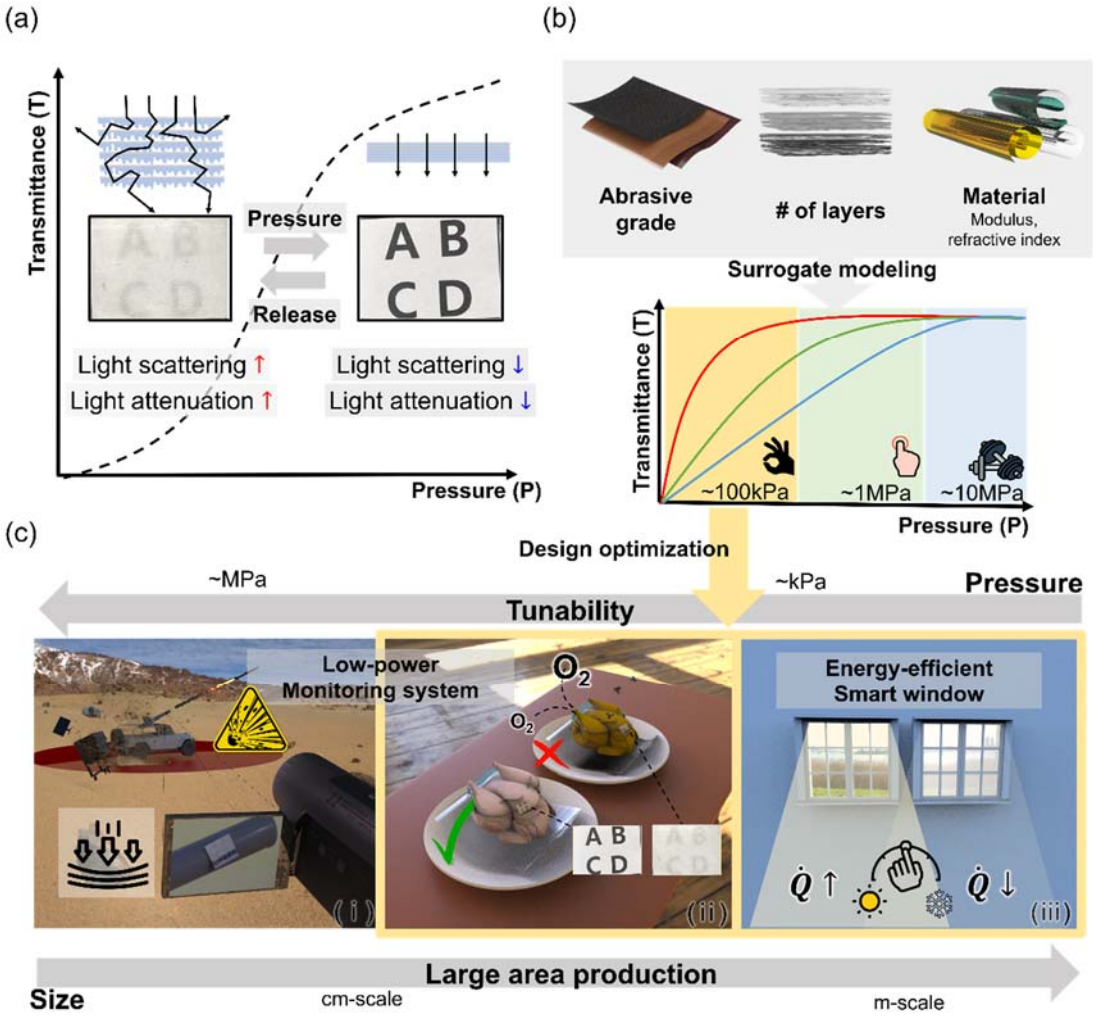

Figure 1. (a) Schematic illustration of PT performance principle of MLHF. (b) Tunability of MLHF. The working range of MLHF could be tuned by modulating abrasive grade, the number of layers, and film material. (c) Schematic illustrations of applications with MLHF: Remote pressure monitoring using a camera with ensuring safety (i) and by eye without energy consumption (ii) and a smart window which modulates optical transmittance for controlling indoor environment conditions (iii). Large area production and tunability of sensitivity are required to MLHF.

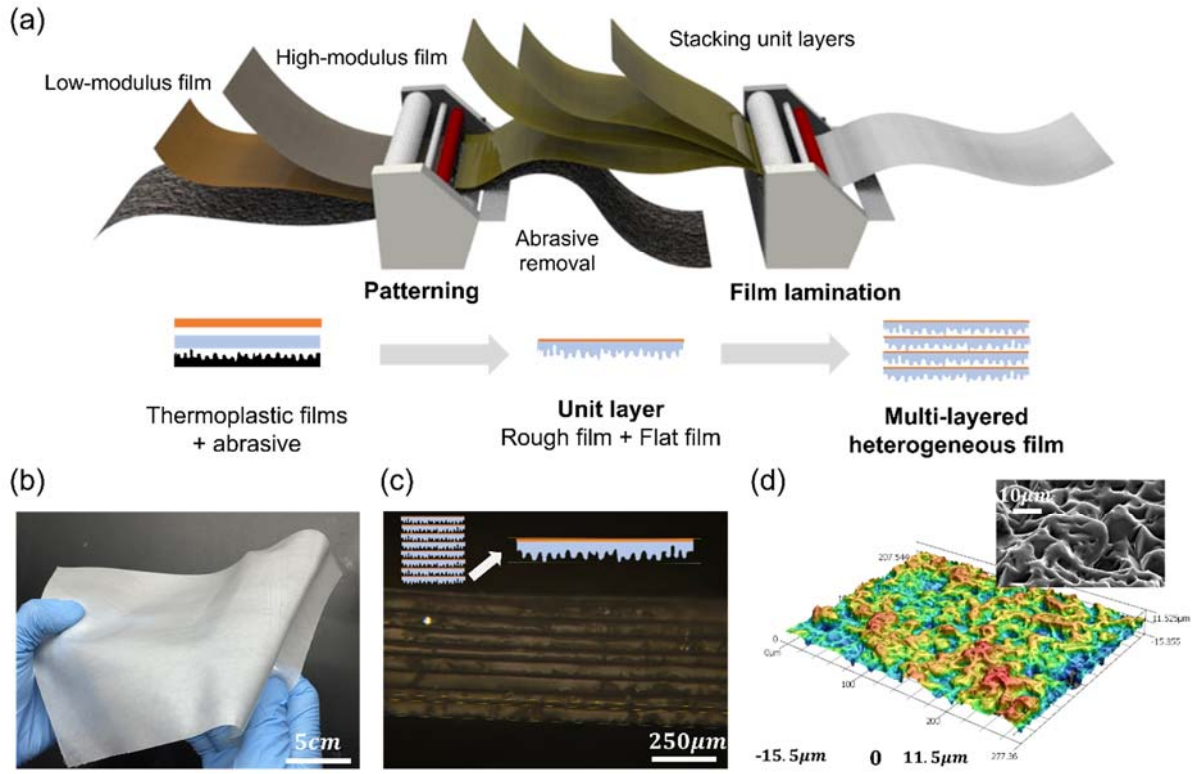

Figure 2. (a) Schematic illustration of the MLHF fabrication process. (b) The MLHF fabrication result is capable of large area production. (c) Microscopy image of a cross-section of MLHF. (d) Confocal microscopy image and SEM image of the rough surface (Grade: P1000).

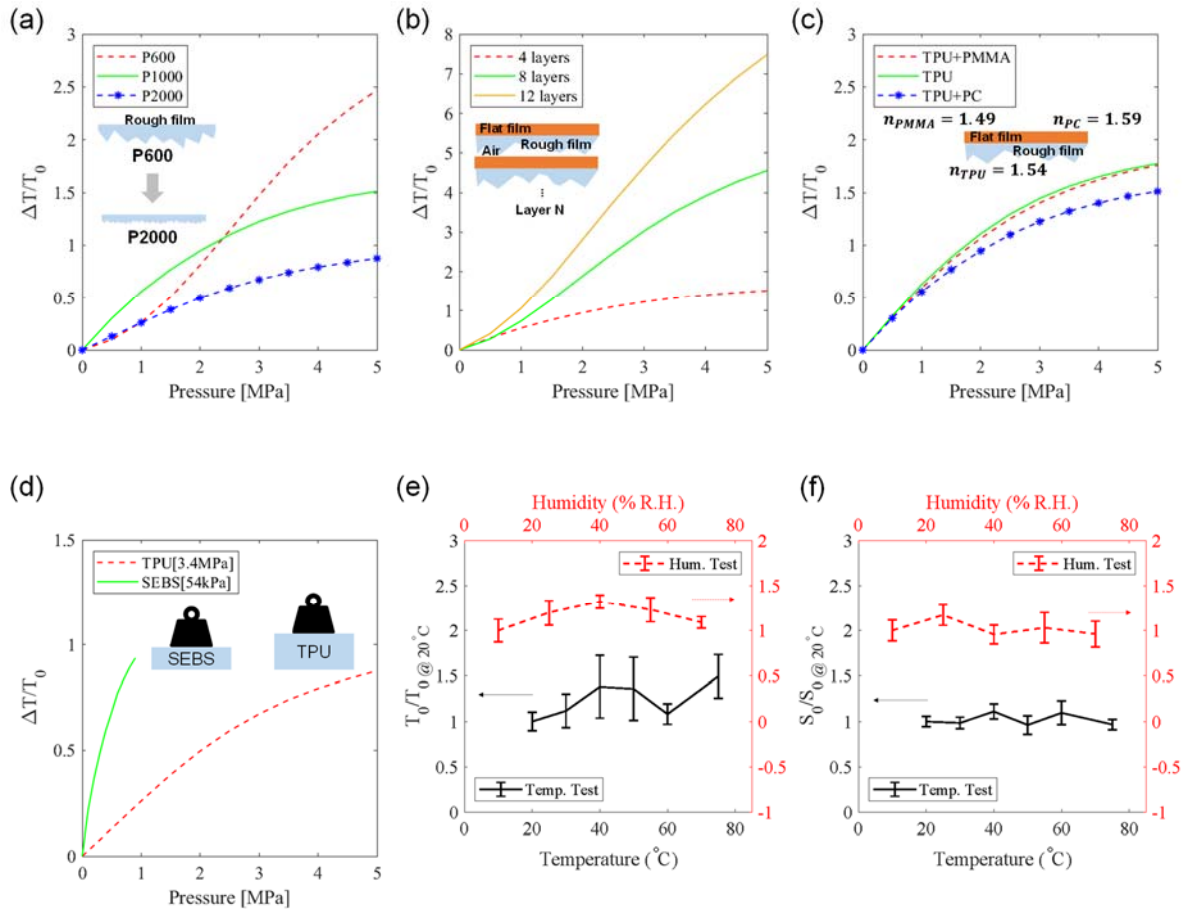

Figure 3. Results of the parameter study which show relative change of transmittance ($\Delta T/T_0$) versus pressure of the MLHF ($\Delta T/T_0$) and environmental test results. (a-d) Results of the parametric study of (a) the grade, (b) the number of layer for P1000, (c) Refractive index, and (d) Young's modulus. The most effective parameter is the Young's modulus. (e-f) Environmental test results of MLHF. ((e) Normalized initial transmittance by initial transmittance of 20℃, and (f) normalized sensitivity by sensitivity of 20℃. The MLHF showed stable performances i.e. initial transmittance and sensitivity in 20-75℃ and 10-70% R.H.

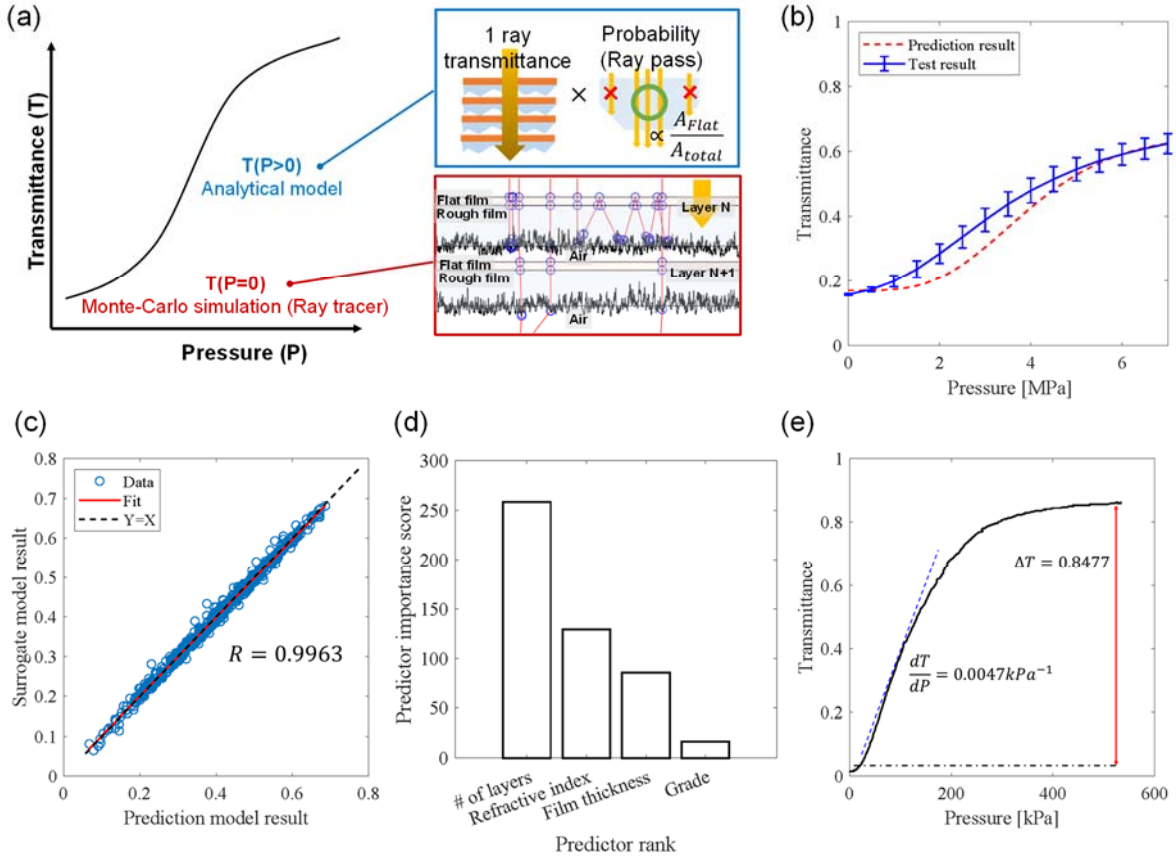

Figure 4 (a) The prediction method of the transmittance for the pressure. Initial transmittance was predicted by the Monte-Carlo simulation with a ray tracer and the remaining transmittances were predicted using the analytical model. (b) Results of the prediction model and compression test. The transmittance of the initial pressure interval tends to be underestimated and the error decreases with increasing pressure. (c) The coefficient of determination (R=0.9963) of the surrogate model using neural network and (d) feature importance results of the surrogate model. The number of layers is the most effective parameter affecting to the sensitivity and transmittance change. (e) PT performance of optimized MLHF with maximized sensitivity ($dT/dP = 0.0047kPa^{-1}$) and transmittance change ($\Delta T = 0.8477$).

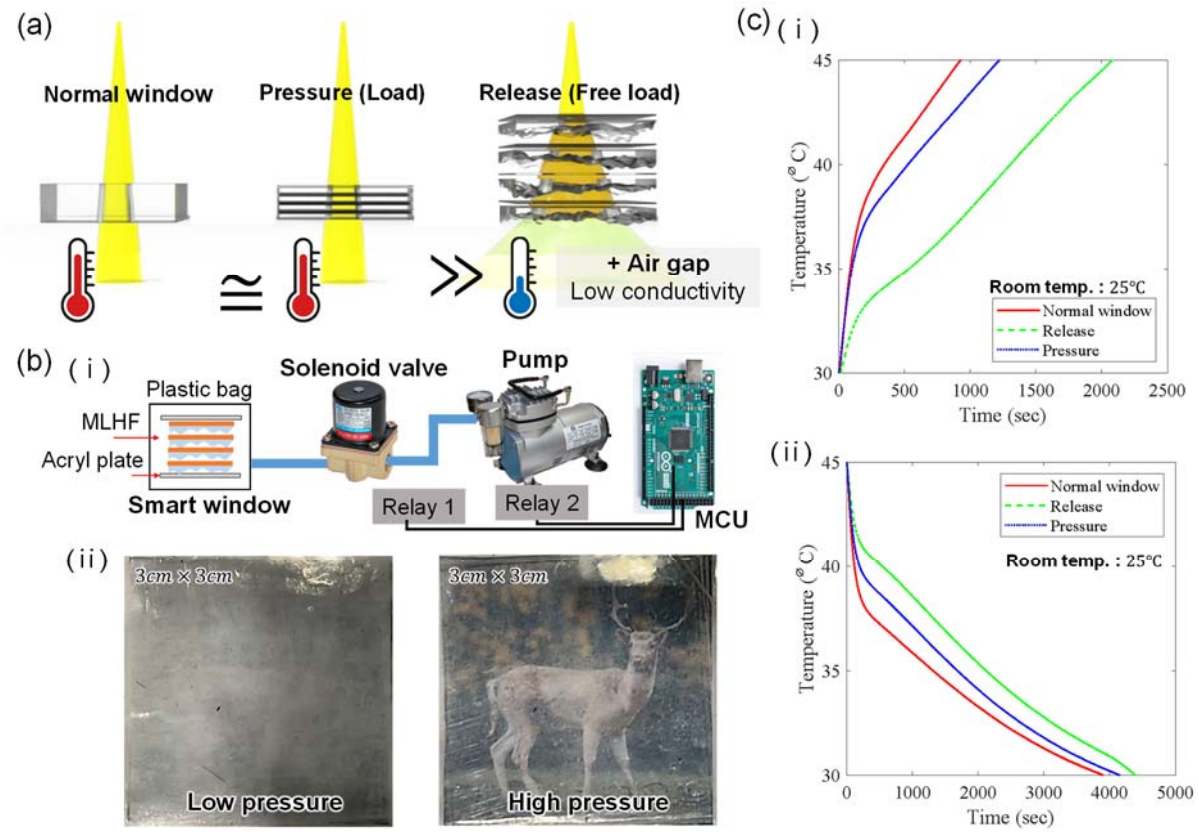

Figure 5. (a) Principle of MLHF operating as smart window. Air gap in the MLHF induce slow thermal conduction and rough surface induce low thermal radiation due to light scattering (b) System configuration of a smart window using hydraulic pump. It is possible to be a low-power system thanks to the solenoid valve. (c) Smart window insulation performance test results in a heating condition (c-i) and a cooling condition (c-ii).

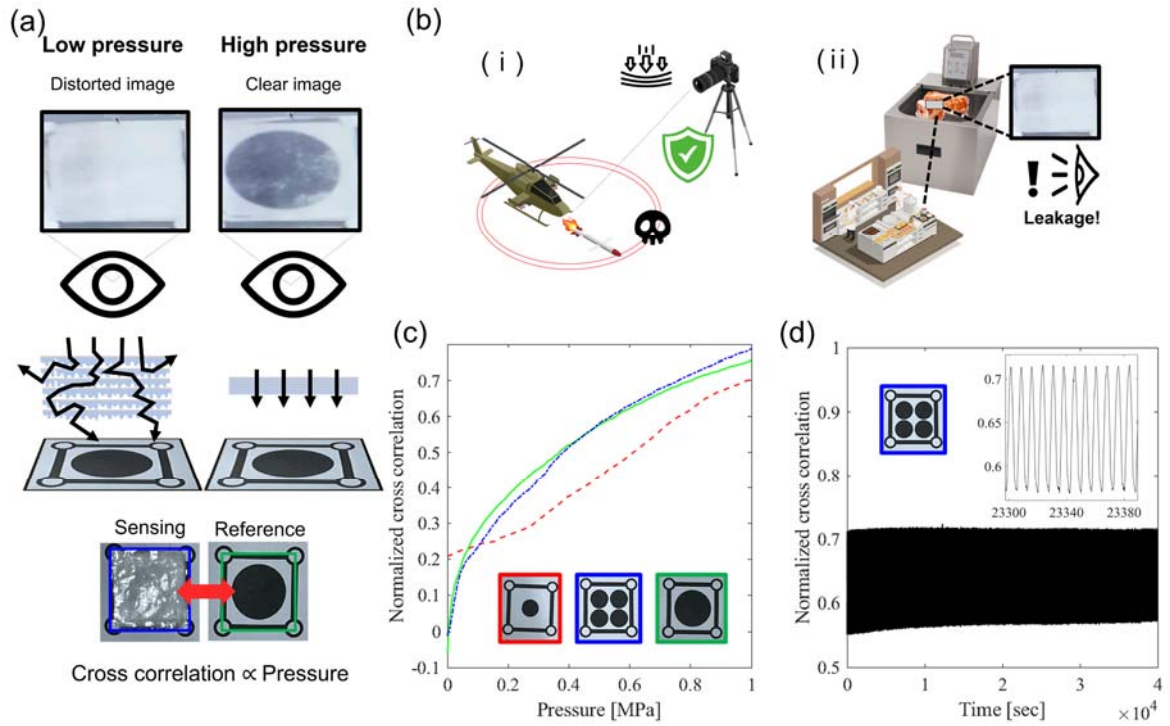

Figure 6. (a) Principle of remote pressure monitoring system containing temperature and humidity indicators. (b) it could be used in harsh environment while protecting equipment and human (i) and measure pressure simply in daily life (ii). (c) tendency according to the type of image. (d) The result of a stability test (4,000 cycles) in the range of P=0.45 −0.8MPa.

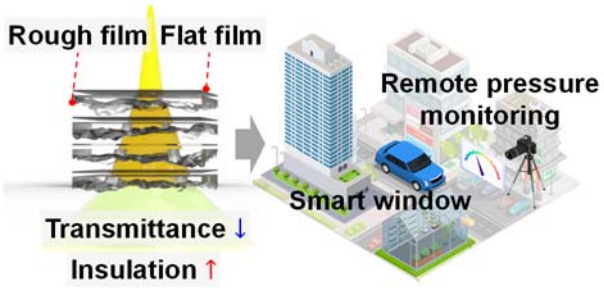

Table of Contents (TOC)